

# Positioning of bound electron wave packets in molecules revealed by high-harmonic spectroscopy

Jing Zhao<sup>†,‡</sup> and Manfred Lein<sup>\*,†</sup>

*Institut für Theoretische Physik and Centre for Quantum Engineering and Space-Time Research (QUEST), Leibniz Universität Hannover, Appelstraße 2, D-30167 Hannover, Germany, and Department of Physics, National University of Defense Technology, Changsha, 410073, China*

---

\*To whom correspondence should be addressed

<sup>†</sup>Institut für Theoretische Physik and Centre for Quantum Engineering and Space-Time Research (QUEST), Leibniz Universität Hannover, Appelstraße 2, D-30167 Hannover, Germany

<sup>‡</sup>Department of Physics, National University of Defense Technology, Changsha, 410073, China

## Abstract

By solution of the time-dependent two-electron Schrödinger equation, we demonstrate that strong-field ionization in combination with electron correlation in molecules can localize bound electron wave packets in molecules. The wave-packet creation is revealed by the emission spectrum in high-order harmonic generation, which is sensitive to the ionization and recombination phase difference between different ionization channels. For hydrogen molecules at stretched internuclear distance, we find that the ionization phase difference between the gerade and ungerade channels is in the range from  $\pi$  and  $1.5\pi$ , indicating that the bound wave packet is initially either on the same side as the outgoing electron or delocalized.

## Introduction

The observation and control of atomic motion in molecules on the femtosecond time scale by using femtosecond laser pulses is a well established area of research.<sup>1</sup> Ongoing efforts have been undertaken to extend ultrafast wave-packet manipulation to electron wave packets on the attosecond time scale.<sup>2</sup> The natural approach to this task is excitation with attosecond pulses,<sup>3</sup> which are formed by high-order harmonic generation (HHG) in laser-irradiated atoms. HHG stands for the conversion of many laser photons into a high-energy photon. It can be understood by the semiclassical three-step model:<sup>4</sup> an electron escapes by tunneling from the highest occupied orbital; the electron is then accelerated in the strong oscillating laser field and may recombine with its parent ion to emit coherent extreme ultraviolet radiation. It has emerged, however, that attosecond processes can be studied without attosecond pulses by analyzing directly the dynamics of atoms and molecules in strong laser fields, *i.e.*, by observing the particles and radiation from laser-irradiated systems.<sup>5,6</sup> A large variety of such molecular imaging methods based on the electron recollision process has been proposed.<sup>7</sup> Particularly HHG has become an important tool to investigate the electronic and geometric structure of molecules<sup>8–14</sup> and ultrafast dynamics.<sup>6,15–17</sup> This is possible because the recombination of an electron and a molecular ion is sensitive to the molecular structure. For instance, HHG spectra from simple two-center molecules exhibit extrema due to structural interference, thus

providing information about the internuclear distance.<sup>18–20</sup> More generally, the correspondence between HHG spectra and photorecombination cross sections has been clearly demonstrated by the success of the quantitative rescattering theory for HHG.<sup>21</sup> The minima observed in HHG spectra from aligned CO<sub>2</sub> molecules, however, depend on the laser intensity,<sup>9,10</sup> indicating that a purely structural explanation is not sufficient. Recent experimental and theoretical work suggests that the involvement of lower-lying molecular orbitals, *i.e.*, multichannel HHG,<sup>13,16</sup> is responsible for the intensity dependence of the minimum position. Tunneling from a lower-lying orbital creates the molecular ion in an excited electronic state and the coherent superposition of electronic states results in bound electron wave-packet dynamics during the second step of HHG.<sup>16</sup> Since HHG with multiple channels must connect the same initial to the same final state of the molecule, it records the information about multielectron dynamics and the rearrangement of electrons upon tunneling ionization. Therefore high-harmonic spectroscopy is capable of resolving correlated electron dynamics with attosecond temporal resolution.<sup>22–26</sup> Interestingly, this approach allows to determine the initial shape and location of the hole left by a tunneling electron. For N<sub>2</sub> molecules, a counter-intuitive phase difference of  $\pi$  between the main ionic states was found,<sup>25</sup> implying an unexpected initial location of the hole, possibly due to electron correlation during tunneling ionization. A theoretical study of the electron-electron interaction during ionization suggests that an attosecond correlation pulse produced by the departing electron facilitates ionization from deeper orbitals.<sup>27</sup>

In this paper, we solve the time-dependent Schrödinger equation to confirm that correlated strong-field ionization processes create bound electron wave packets. As a model, we employ a one-dimensional H<sub>2</sub> molecule with fixed nuclei. We develop a method to determine the initial shape of the remaining bound electron wave packet and thus the ionization phase. In their pioneering work, Smirnova and coworkers have assumed the ionization phase to be 0 or  $\pi$  to reproduce the experimental harmonic spectra.<sup>16,25</sup> In our study, we investigate the dependence of the phase on the internuclear distance and the laser intensity. We show that the location of the hole left by tunnel ionization can be manipulated by varying the laser intensity. Although the intuitive picture of ionization from lower-lying orbitals does not readily apply in the case of H<sub>2</sub> with its doubly

occupied Hartree-Fock orbital, it is still possible to assign different Dyson orbitals to the different ionization channels, which correspond to the electronic states of the  $\text{H}_2^+$  ion. The internuclear distance is chosen larger than the equilibrium distance in order to make the energy gap between the ground and first excited states of the ion comparable with the laser frequency, so that the electronic rearrangement dynamics occurs on the sub-laser-cycle time scale and influences the HHG spectrum.<sup>16</sup> We show that a double-channel HHG model using the numerically calculated time-dependent ionization phase partially explains the extrema in the HHG spectrum. These extrema cannot be understood in a single-channel picture.

## 1D Model

The time-dependent Schrödinger equation (TDSE) for the two-electron wave function  $\Psi(x_1, x_2, t)$  describing 1D  $\text{H}_2$  in a laser field  $E(t)$  reads (atomic units are used)

$$i\partial_t\Psi(x_1, x_2, t) = \left[ -\frac{\partial_1^2}{2} - \frac{\partial_2^2}{2} + V(x_1, x_2) + (x_1 + x_2)E(t) \right] \Psi(x_1, x_2, t) \quad (1)$$

where  $V(x_1, x_2) = U(x_1) + U(x_2) + W(x_1 - x_2)$  with  $U(x) = -W(x - R/2) - W(x + R/2)$  and  $W(x) = (x^2 + 1)^{-\frac{1}{2}}$ . Trapezoidally shaped 1200 nm laser pulses with a total duration of 4 optical cycles and linear ramps of one optical cycle are used. The time evolution starts from the ground state which is obtained by imaginary-time propagation. The split-operator method<sup>28</sup> is applied to solve the TDSE with 2048 time steps per optical cycle. The HHG spectrum is obtained as the Fourier transform of the time-dependent dipole acceleration,<sup>29</sup> *i.e.*,

$$S(\omega) \sim \left| \int \langle \Psi(t) | (\partial_1 + \partial_2)V + 2E(t) | \Psi(t) \rangle e^{i\omega t} dt \right|^2. \quad (2)$$

For comparison, we consider also a laser-field-free setup, in which harmonics are generated by collision of a Gaussian electron wave packet that is initially prepared heading towards the molecular ion in the ground state. The continuous emission spectrum from the collision shows the effect

of molecular structure on HHG in the absence of multichannel effects or distortions due to the laser field. We use the wave-packet collision instead of a heuristic formula<sup>19</sup> in order to include Coulomb effects exactly in the determination of the structural effects. The initial state for this calculation is a superposition of the two-electron ground state  $\Psi_0(x_1, x_2)$  and a symmetrized product of the ionic ground state  $\varphi_g(x)$  with a Gaussian wave packet  $\psi_G(x)$ ,

$$\Psi(x_1, x_2) = \alpha \Psi_0(x_1, x_2) + \beta S[\varphi_g(x_1) \psi_G(x_2)], \quad (3)$$

where  $S$  is the symmetrization operator for the two coordinates  $x_1, x_2$ . The Gaussian wave packet  $\psi_G(x) = \exp(-(x - x_0)^2/(2\sigma^2) + ikx)$  is initially centered at  $x_0 = 80$  a.u. with  $\sigma = 0.3$  a.u., moving with a central momentum  $k = -1.3$  a.u. toward the molecular ion. We set  $\alpha/\beta = 10^3$  to mimic an HHG process in a weakly ionized system.

## Results and Discussion

The HHG spectra at various internuclear distances are shown in Figure 1 in comparison with the smooth HHG spectra from the wave-packet collision. At small internuclear distances ( $R = 1.4$  a.u. and  $R = 2$  a.u.), we find that the minimum in the collision spectrum occurs at the same frequency as in laser-induced HHG. This shows that the suppression of the harmonic intensity is a purely structural effect. Indeed it originates from destructive two-center interference.<sup>18-20</sup> As the internuclear distance is increased, the energy gap  $\Delta E$  between the ionic ground state and first excited state is reduced ( $R = 5.2$  a.u.,  $\Delta E = 0.0566$  a.u.;  $R = 6$  a.u.,  $\Delta E = 0.0302$  a.u.). Therefore, ionization to the excited ionic state may start to play a role. As can be seen from Figures 1(c) and (d), the minima in the collision spectra appear at frequencies different from the laser-induced spectra. This demonstrates that ionization to the ionic ground state is not sufficient to explain HHG at increased distance.

To investigate the strong-field ionization process in more detail, we consider  $H_2$  interacting with a half-cycle pulse. The two-electron density  $|\Psi(x_1, x_2, t)|^2$  at the peak of the half-cycle pulse

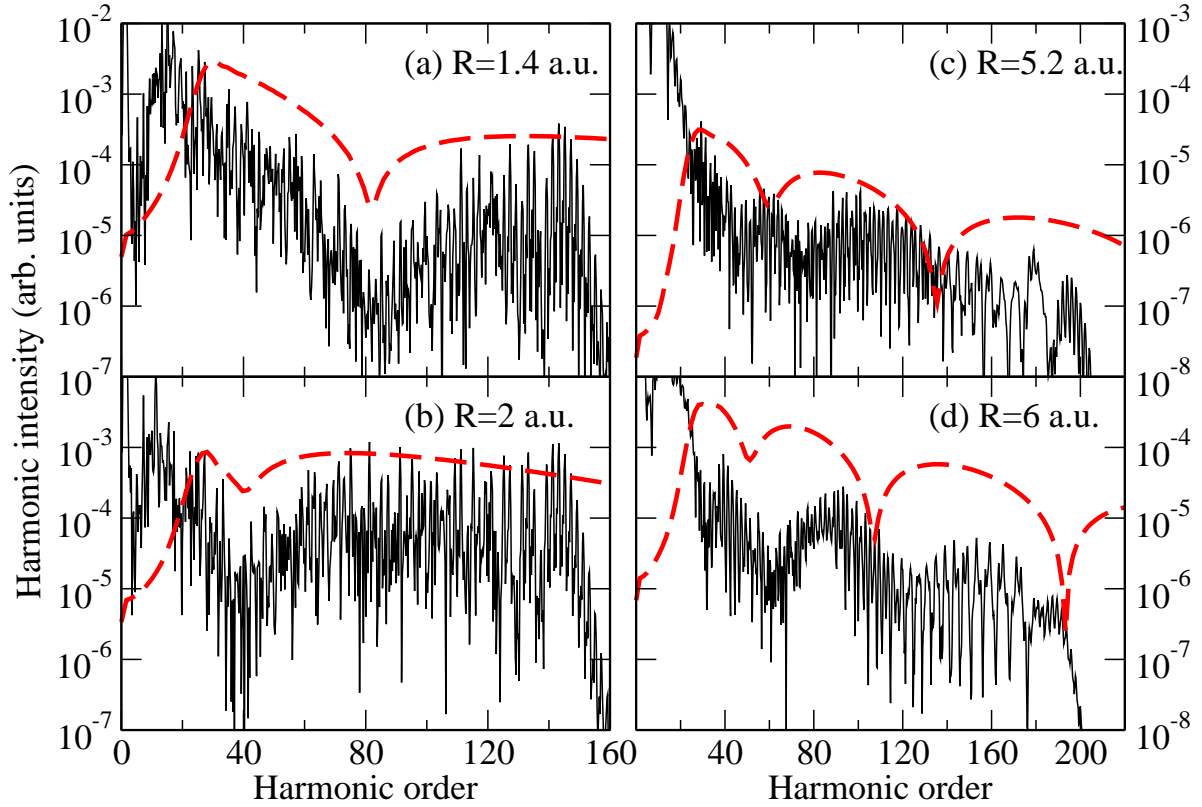


Figure 1: (Color online) HHG spectra for 1D  $H_2$  at various internuclear distances. The laser intensity is  $3 \times 10^{14} \text{ W/cm}^2$  in (a),(b) and  $4 \times 10^{14} \text{ W/cm}^2$  in (c),(d). Dashed lines: spectra emitted by collision of a Gaussian wave packet with the molecular ion.

(with positive electric field) is shown in Figure 2 for  $R=6 \text{ a.u.}$  using two different laser intensities. The major part of the density resides in a ground-state-like part with the two electrons located on opposite sides of the molecule. Additionally, there is density escaping towards negative values of  $x_1$  or  $x_2$ , representing single ionization. For the lower intensity, we see that both electron coordinates are negative in the ionizing part, *i.e.*, ionization localizes the remaining bound electron at the site that is on the same side as the outgoing electron. For the higher intensity, the coordinate of the bound electron can be positive or negative, indicating delocalization of the remaining electron.

In order to obtain a more quantitative description, we calculate the wave function of the bound electron. First, the bound wave packet  $\varphi(x_1, k, t)$  at time  $t$  after the half-cycle pulse for outgoing electron momentum  $k$  is obtained as the overlap between the two-electron wave function and the

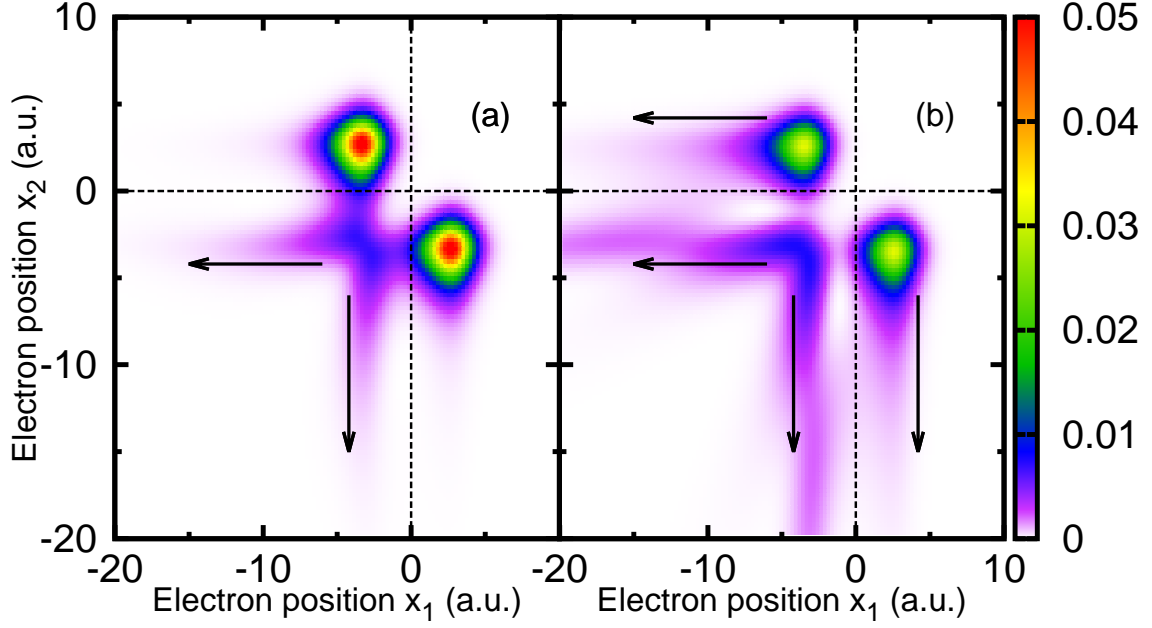


Figure 2: (Color online) Two-electron density at the peak of a half-cycle pulse for  $R = 6$  a.u. (a) Laser intensity  $2 \times 10^{14}$  W/cm<sup>2</sup>. (b) Laser intensity  $4 \times 10^{14}$  W/cm<sup>2</sup>.

outgoing electron approximated as a plane wave, *i.e.*,

$$\varphi(x_1, k, t) = \int e^{-ikx_2} w(x_2) \Psi(x_1, x_2, t) dx_2. \quad (4)$$

We use a window function  $w(x) = \frac{1}{1+e^{5(x+10)}} + \frac{1}{1+e^{5(-x+10)}}$  to eliminate the inner part of the wave function, where the ground state is located. We relate the momentum of the outgoing electron to the ionization time  $t_i$  by the classical expression  $k = -\int_{t_i}^t E(t') dt'$ . The bound wave packet is propagated backwards in time using the one-electron TDSE with the same half-cycle pulse as in the two-electron TDSE, yielding the initial bound wave packet  $\chi(x_1, t_i)$  at the ionization time  $t_i$ . Since the tunnel ionization rate is exponentially sensitive to the ionization energy, we only consider the two most important channels, namely the  $H_2^+$  ion in the gerade ground state  $\varphi_g$  or ungerade first excited state  $\varphi_u$ . For every ionization time, we calculate the populations  $|C_{g,u}|^2$  of the two states and their relative phase  $\phi = \arg(C_u/C_g)$  from the complex amplitudes  $C_{g,u} = \langle \varphi_{g,u} | \chi(t_i) \rangle$ . Our convention for the ionization phase  $\phi$  is that  $\phi = 0$  refers to the bound electron located opposite to the outgoing electron. This is in accordance with the definition in the

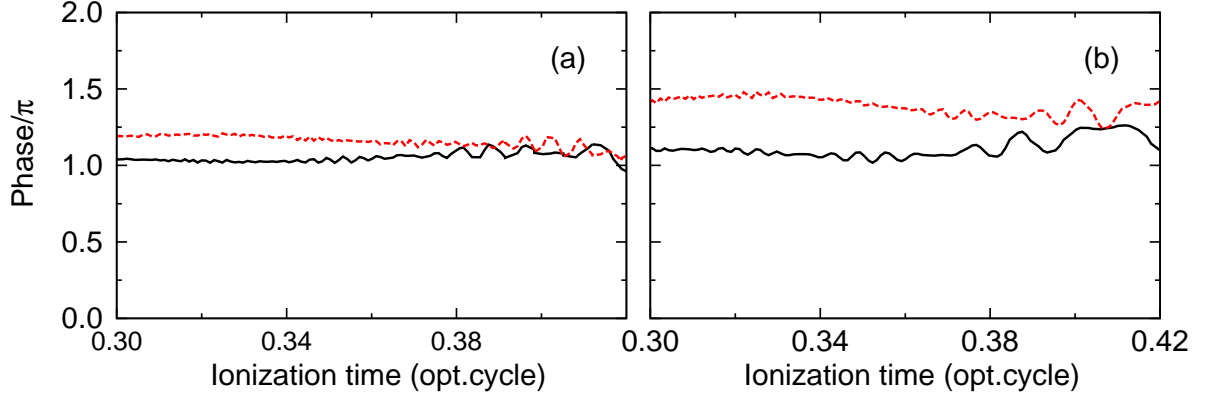


Figure 3: (Color online) Relative phase between the ungerade and gerade states versus ionization time. Solid lines: intensity  $2 \times 10^{14}$  W/cm<sup>2</sup>. Dashed lines: intensity  $4 \times 10^{14}$  W/cm<sup>2</sup>. Left panel:  $R = 5.2$  a.u. Right panel:  $R = 6$  a.u.

work by Smirnova and coworkers, where the ionization phase refers to the phase difference of the ionizing wings of different Dyson orbitals.

The two states are found to be almost equally populated for the internuclear distances  $R = 5.2$  a.u. and  $R = 6$  a.u. Figure 3 shows that the ionization phase depends on the laser intensity, especially when the internuclear distance is large. This indicates that the location of the ionization-induced hole depends on the laser intensity as well. The ionization phase depends weakly on the ionization time. For the lower intensity  $2 \times 10^{14}$  W/cm<sup>2</sup>, the phase stays close to  $\pi$ , *i.e.*, the bound electron starts on the same side as the outgoing electron. This is consistent with the mechanism of enhanced ionization via the ion-pair state.<sup>30</sup> For the higher intensity  $4 \times 10^{14}$  W/cm<sup>2</sup> and  $R = 6$  a.u., the phase is near  $3\pi/2$ . Phases far from 0 and  $\pi$  imply a delocalized wave packet in the process of moving from one nucleus to the other. Varying the laser intensity allows us to vary the phase, therefore opening a possibility for controlling the electron localization.

As shown in Ref. 25, the ionization phase is encoded in the HHG spectrum. To extract this information, we introduce a recollision model for describing the extrema in the HHG spectrum. The essential ingredients of the model are the ionization phase, the bound-electron motion, and the recombination phase. We assume that at times  $t$  close to recollision, the system is in a superposition of the two-electron ground state  $\Psi_0(x_1, x_2, t) = \Psi_0(x_1, x_2)e^{-iE_0t}$  and a symmetrized product of a

bound ionic wave packet  $\psi^+$  with a continuum wave packet  $\psi_c(x, t)$ ,

$$\Psi(x_1, x_2, t) = \alpha \Psi_0(x_1, x_2, t) + \beta S[\psi^+(x_1, t)\psi_c(x_2, t)]. \quad (5)$$

If the two ionic states are equally populated and if there is no laser-induced excitation between ionization and recombination, the ionic wave packet is

$$\psi^+(x, t) = \left( \varphi_g(x) + \varphi_u(x) e^{-i\omega\tau + i\phi} \right) e^{-iE_g\tau} \quad (6)$$

with  $\omega = \Delta E$  and  $E_g$  being the  $H_2^+$  ground-state energy. However, in the presence of the laser field, we deduce from our calculations that the wave packets oscillate approximately with the laser frequency and therefore we set  $\omega$  equal to the laser frequency. The travel time  $\tau = t - t_i$  determines the dynamical phase  $\omega\tau$  accumulated after ionization. The molecular ground state at large internuclear separation is well approximated by the Heitler-London-type function

$$\Psi_0(x_1, x_2) = \frac{1}{\sqrt{2}} (\varphi_g(x_1)\varphi_g(x_2) - \varphi_u(x_1)\varphi_u(x_2)). \quad (7)$$

The Dyson orbitals corresponding to the ionic states  $\varphi_g$  and  $\varphi_u$  are then  $D_g = \sqrt{2}\langle\varphi_g|\Psi_0\rangle = \varphi_g$  and  $D_u = \sqrt{2}\langle\varphi_u|\Psi_0\rangle = -\varphi_u$ . The emission spectrum  $S(\Omega)$  is proportional to the modulus squared of the Fourier transform of the dipole-velocity expectation value<sup>31</sup>

$$v_d(t) = i\langle\Psi(t)|\partial_1 + \partial_2|\Psi(t)\rangle. \quad (8)$$

Setting the continuum wave packet to a plane wave  $\psi_c(x, t) = e^{ikx - iE_k t}$  with momentum  $k$ , using linear combinations of atomic orbitals for the states  $\varphi_g$  and  $\varphi_u$ , keeping only continuum-bound transitions, and neglecting exchange contributions<sup>32</sup> leads (within a temporal saddle-point approximation) to the result

$$S(\Omega) \sim 1 - \sin(|k|R) \sin(\omega\tau - \phi). \quad (9)$$

We have assumed that the excited-state channel has the same trajectories as the ground state (neglecting the difference in ionization energy) and we have used that the recombination matrix elements for the gerade and ungerade states differ by a phase of  $\pi/2$ . The harmonic photon energy  $\Omega$  is the sum of the kinetic recollision energy and the ionization potential  $I_p$ , *i.e.*,  $\Omega = E_k + I_p$ . The travel time  $\tau$  is obtained classically using the short trajectory.<sup>33</sup> We evaluate the interference pattern predicted by Eq. (9) using the numerically obtained ionization phase  $\phi$  from Figure 3. To this end, the ionization time is mapped to harmonic order according to the classical recollision model.<sup>4</sup>

In addition to the HHG spectra we calculate the time-frequency distribution<sup>34</sup> using the Gabor transform.<sup>35</sup> The results are shown in Figure 4 and Figure 5 for two different laser intensities. Figures 4(a),(b) show clear minima in the short trajectory at intermediate harmonic orders, namely at about harmonic 69 in Figure 4(a) and harmonic 57 in Figure 4(b). In the HHG spectra, these minima are visible, but less pronounced due to the summation over short and long trajectories. Using the recollision model with the ionization phase from Figure 3, these minima are well reproduced. At the same orders, there is no interference minimum in the long trajectory, showing clearly the sensitivity to the electron travel time, which is expected in multichannel interference. The model does not reproduce well the minimum at the lower harmonic order 40 in Figure 4(c). This may be due to a low-energy failure of the model, which is based on plane waves and Coulomb-free trajectories. In general, however, the model reproduces the features of the numerical calculations well. This is seen also for the higher laser intensity in Figure 5. The structures in the short trajectory in the range  $-4\text{fs} < t < -2\text{fs}$  in Figures 5(a),(b) are consistent with the model. The signal at earlier times comes from the rising edge of the laser pulse and should not be compared to the model. For  $R = 6\text{ a.u.}$ , the model now uses a phase significantly above  $\pi$ , see Figure 3(b). Choosing the phase constant and equal to zero or  $\pi$  does not satisfactorily reproduce the numerical result. This is apparent by inspection of the minimum at harmonic order 125 in Figure 5(d). Only the correct choice of phase in the interference model reproduces the minima. The HHG spectrum thus provides the information on the electron localization. This method of observing the electron dynamics can be adapted to more complex systems once the electronic states and transition matrix elements

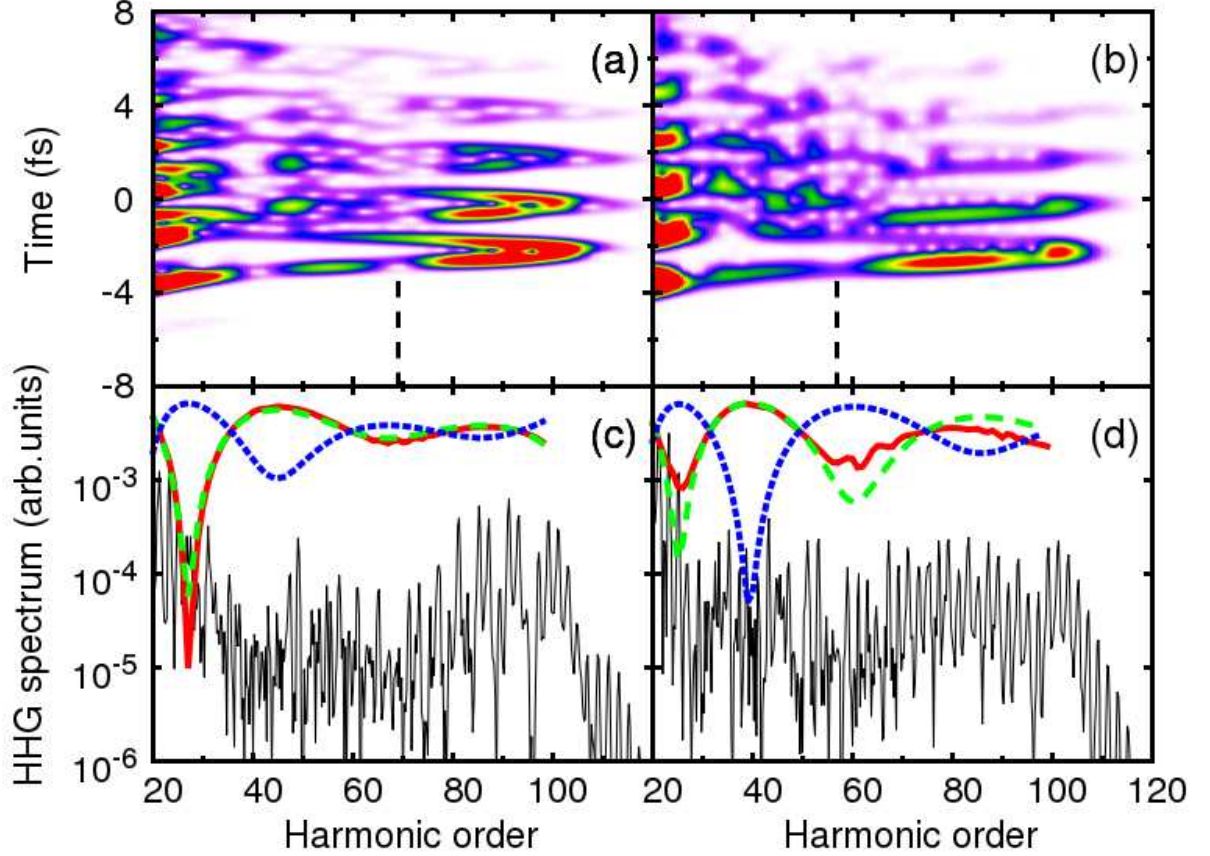


Figure 4: (Color online) Time-frequency analysis and HHG spectra of  $\text{H}_2$  for the laser intensity  $2 \times 10^{14} \text{ W/cm}^2$ . Also shown are the emission spectra obtained using the recollision model, Eq. (9), with the ionization phase from Figure 3 (thick solid lines),  $\phi = \pi$  (thick dashed lines) and  $\phi = 0$  (thick dotted lines). Left panel:  $R = 5.2 \text{ a.u.}$  Right Panel:  $R = 6 \text{ a.u.}$

are known.

## Conclusion

In summary, we have provided numerical evidence for bound wave-packet creation by strong-field ionization of two-electron molecules. The location of the initial wave packet can be controlled by varying the laser intensity. A simple recollision model has been applied to predict how the positions of interference minima in the HHG spectrum depend on the wave packet localization. The model shows good agreement with the numerical TDSE results provided that the correct ionization phase,

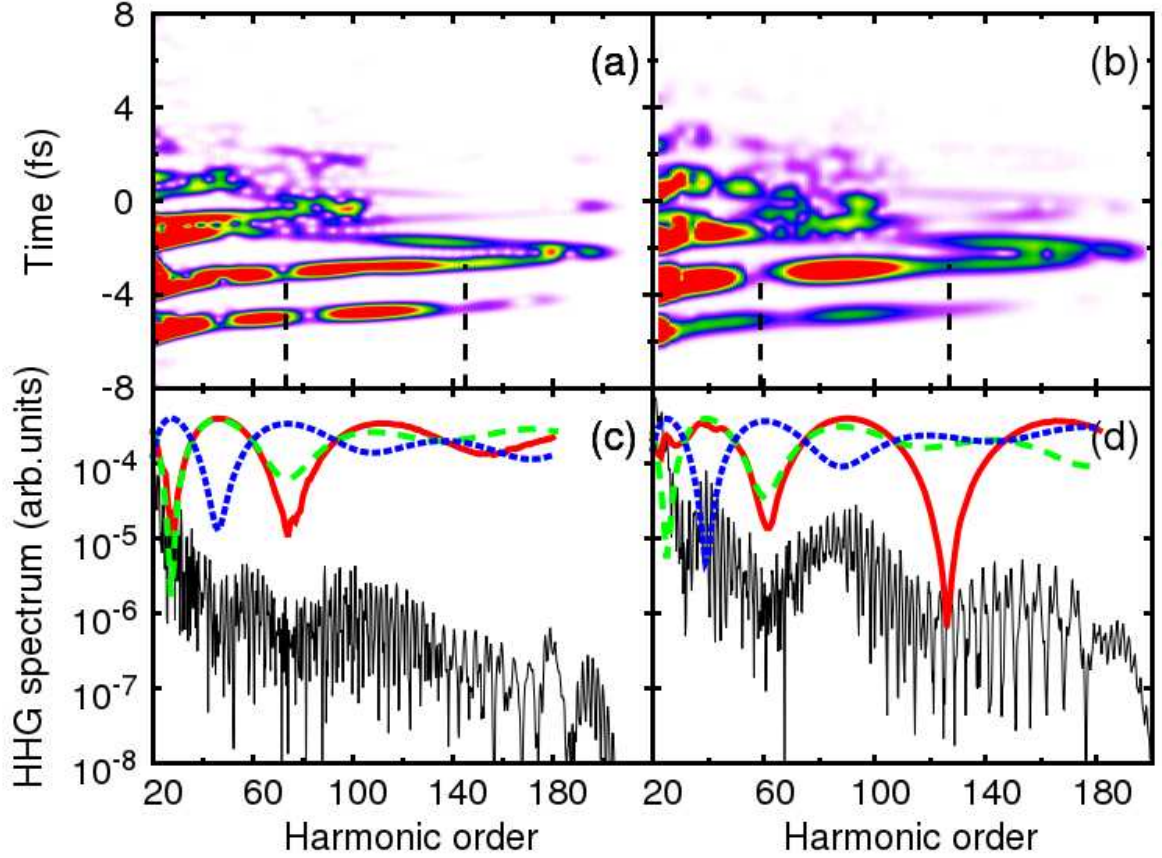


Figure 5: Same as Figure 4 but for the intensity  $4 \times 10^{14} \text{ W/cm}^2$ .

*i.e.*, the correct initial wave-packet location, is used. Our finding demonstrates the power of high-harmonic spectroscopy for molecular imaging on the subfemtosecond and Ångström scale. It may provide a new possibility for experimental investigation of ionization mechanisms such as the ion-pair-type enhanced ionization of  $\text{H}_2$ .

## Acknowledgement

We thank the Deutsche Forschungsgemeinschaft for funding the Centre for Quantum Engineering and Space-Time Research (QUEST). J. Zhao acknowledges support from the China Scholarship Council (CSC). M. Lein thanks A. Saenz for valuable discussions.

## References

- (1) (a) Zewail, A. H. *J. Phys. Chem. A* **2000**, *104*, 5660. (b) Assion; A. *et al. Science* **1998**, *282*, 919. (c) Wollenhaupt, M.; Engel, V.; Baumert, T. *Ann. Rev. Phys. Chem.* **2005**, *56*, 25.
- (2) Krausz, F.; Ivanov, M. *Rev. Mod. Phys.* **2009**, *81*, 163.
- (3) Chang, Z.; Corkum, P. J. *Opt. Soc. Am. B* **2010**, *27*, B9.
- (4) Corkum, P. B. *Phys. Rev. Lett.* **1993**, *71*, 1994.
- (5) Niikura, H.; Légaré, F.; Hasbani, R.; Ivanov, M. Y.; Villeneuve, D. M.; Corkum, P. B. *Nature* **2003**, *421*, 826.
- (6) Baker, S.; Robinson, J. S.; Haworth, C. A.; Teng, H.; Smith, R. A.; Chirilă, C. C.; Lein, M.; Tisch, J. W. G.; Marangos, J. P. *Science* **2006**, *312*, 424.
- (7) Lein, M. *Journal of Physics B* **2007**, *40*, R135.
- (8) Itatani, J.; Levesque, J.; Zeidler, D.; Niikura, H.; Pepin, H.; Kieffer, J. C.; Corkum, P. B.; Villeneuve, D. M. *Nature* **2004**, *432*, 867.
- (9) Kanai, T.; Minemoto, S.; Sakai, H. *Nature* **2005**, *435*, 470.
- (10) Vozzi, C.; Calegari, F.; Benedetti, E.; Caumes, J.-P.; Sansone, G.; Stagira, S.; Nisoli, M.; Torres, R.; Heesel, E.; Kajumba, N.; Marangos, J. P.; Altucci, C.; Velotta, R. *Phys. Rev. Lett.* **2005**, *95*, 153902.
- (11) Boutu, W.; Haessler, S.; Merdji, H.; Breger, P.; Waters, G.; Stankiewicz, M.; Frasiniski, L. J.; Taieb, R.; Caillat, J.; Maquet, A.; Monchicourt, P.; Carre, B.; Salieres, P. *Nat. Phys.* **2008**, *4*, 545.
- (12) Zhao, J.; Zhao, Z. *Phys. Rev. A* **2008**, *78*, 053414.
- (13) McFarland, B. K.; Farrell, J. P.; Bucksbaum, P. H.; Gühr, M. *Science* **2008**, *322*, 1232.

- (14) Haessler, S.; Caillat, J.; Boutu, W.; Giovanetti-Teixeira, C.; Ruchon, T.; Auguste, T.; Divveki, Z.; Breger, P.; Maquet, A.; Carré, B.; Taïeb, R.; Salières, P. *Nat. Phys.* **2010**, *6*, 200.
- (15) Baker, S.; Robinson, J. S.; Lein, M.; Chirilă, C. C.; Torres, R.; Bandulet, H. C.; Comtois, D.; Kieffer, J. C.; Villeneuve, D. M.; Tisch, J. W. G.; Marangos, J. P. *Phys. Rev. Lett.* **2008**, *101*, 053901.
- (16) Smirnova, O.; Mairesse, Y.; Patchkovskii, S.; Dudovich, N.; Villeneuve, D.; Corkum, P.; Ivanov, M. Y. *Nature* **2009**, *460*, 972.
- (17) Bredtmann, T.; Chelkowski, S.; Bandrauk, A. D. *Phys. Rev. A* **2011**, *84*, 021401(R).
- (18) Lein, M.; Hay, N.; Velotta, R.; Marangos, J. P.; Knight, P. L. *Phys. Rev. Lett.* **2002**, *88*, 183903.
- (19) Lein, M.; Hay, N.; Velotta, R.; Marangos, J. P.; Knight, P. L. *Phys. Rev. A* **2002**, *66*, 023805.
- (20) Lagmago Kamta, G.; Bandrauk, A. D. *Phys. Rev. A* **2005**, *71*, 053407.
- (21) Le, A.-T.; Lucchese, R. R.; Tonzani, S.; Morishita, T.; Lin, C. D. *Phys. Rev. A* **2009**, *80*, 013401.
- (22) Smirnova, O.; Patchkovskii, S.; Mairesse, Y.; Dudovich, N.; Ivanov, M. Y. *Proceedings of the National Academy of Sciences* **2009**, *106*, 16556.
- (23) Smirnova, O.; Ivanov, M. *Nat. Phys.* **2010**, *6*, 159.
- (24) Wörner, H. J.; Bertrand, J. B.; Hockett, P.; Corkum, P. B.; Villeneuve, D. M. *Phys. Rev. Lett.* **2010**, *104*, 233904.
- (25) Mairesse, Y.; Higuët, J.; Dudovich, N.; Shafir, D.; Fabre, B.; Mével, E.; Constant, E.; Patchkovskii, S.; Walters, Z.; Ivanov, M. Y.; Smirnova, O. *Phys. Rev. Lett.* **2010**, *104*, 213601.

- (26) Torres, R.; Siegel, T.; Brugnera, L.; Procino, I.; Underwood, J. G.; Altucci, C.; Velotta, R.; Springate, E.; Froud, C.; Turcu, I. C. E.; Patchkovskii, S.; Ivanov, M. Y.; Smirnova, O.; Marangos, J. P. *Phys. Rev. A* **2010**, *81*, 051802.
- (27) Walters, Z. B.; Smirnova, O. *J. Phys. B* **2010**, *43*, 161002.
- (28) Feit, M.; Jr., J. F.; Steiger, A. *J. Comput. Phys.* **1982**, *47*, 412.
- (29) Burnett, K.; Reed, V. C.; Cooper, J.; Knight, P. L. *Phys. Rev. A* **1992**, *45*, 3347.
- (30) (a) Saenz, A. *Phys. Rev. A* **2000**, *61*, 051402(R). (b) Saenz, A. *Phys. Rev. A* **2002**, *66*, 063407.
- (31) Chirilă, C. C.; Lein, M. *J. Mod. Opt.* **2007**, *54*, 1039.
- (32) (a) Santra, R.; Gordon, A. *Phys. Rev. Lett.* **2006**, *96*, 073906. (b) Patchkovskii, S; Zhao, Z; Brabec, T; Villeneuve, D. M. *Phys. Rev. Lett.* **2006** *97*, 123003.
- (33) Lewenstein, M.; Balcou, Ph.; Ivanov, M. Yu.; L'Huillier, A.; Corkum, P. B. *Phys. Rev. A* **1994**, *49*, 2117.
- (34) Antoine, P.; Piraux, B.; Maquet, A. *Phys. Rev. A* **1995**, *51*, R1750.
- (35) Chirilă, C. C.; Dreissigacker, I.; van der Zwan, E. V.; Lein, M. *Phys. Rev. A* **2010**, *81*, 033412.